HHS Public Access

Author manuscript

Invest New Drugs. Author manuscript; available in PMC 2020 April 01.

Published in final edited form as:

Invest New Drugs. 2019 April ; 37(2): 364–374. doi:10.1007/s10637-018-0647-0.

Development of Apratoxin S10 (Apra S10) as an Anti-pancreatic Cancer Agent and Its Preliminary Evaluation in an Orthotopic Patient-derived Xenograft (PDX) Model

Weijing Cai[1,2], **Ranjala Ratnayake**[1,2], **Michael H. Gerber**[3], **Qi-Yin Chen**[1,2], **Yichao Yu**[4], **Hartmut Derendorf**[4], **Jose G. Trevino**[3], and **Hendrik Luesch**[*,1,2]

[1]Department of Medicinal Chemistry, College of Pharmacy, University of Florida, Gainesville, Florida 32610, USA

[2]Center for Natural Products, Drug Discovery and Development (CNPD3), University of Florida, Gainesville, Florida 32610, USA

[3]Department of Surgery, College of Medicine, University of Florida, Gainesville, Florida 32610, USA

[4]Department of Pharmaceutics, College of Pharmacy, University of Florida, Gainesville, Florida 32610, USA

Abstract

Despite the significant progress in the field of cancer therapeutics, the incidence of pancreatic cancer (PC) has continuously increased. One possible mechanism for this increasing burden is impaired drug delivery and drug resistance resulting from a unique tumor microenvironment and genetic mutations. Apratoxins are potent anticancer agents and cotranslational translocation inhibitors with potential therapeutic applications to treat cancers with active secretory pathways. Here, we developed apratoxin S10 (Apra S10) as an anti-pancreatic cancer agent which potently inhibited the growth of both established and patient-derived primary pancreatic cancer cells. We validated its mechanism of action on pancreatic cancer cells by demonstrating the downregulation of multiple receptor tyrosine kinases and inhibition of growth factor and cytokine secretion. Apra S10 also inhibited a number of cytokines from stromal cells, suggesting that Apra S10 not only inhibited pancreatic cancer cell secretion, but also reduced the level of factors secreted by other cell types active within the tumor microenvironment. As Apra S10 tissue distribution indicated its high enrichment in pancreas tissue, an orthotopic pancreatic patient-derived xenograft mouse

[*]Corresponding Author luesch@cop.ufl.edu. Phone number: 1-352-273-7738.

Author information

W.C., experimental design, tissue distribution and PK study in mice, LC-MS/MS analysis, efficacy study in mice and manuscript writing; R.R. experimental design for in vitro assays (viability, RTKs, cytokine profiling) and edited manuscript; M.H.G., in vivo study and edited manuscript; J.G.T., supervised in vivo studies. Q.Y.C., scale-up total synthesis. Y.Y., PK parameter analysis and simulation study; H.D., supervised PK parameter analysis and simulation study. H.L., designed and supervised the study and edited the manuscript.

Compliance with ethical standards

Ethical approval

All applicable international, national, and /or institutional guidelines for the care and use of animals were followed.

Conflict of interest

The authors declare the following competing financial interest(s): H. Luesch is co-founder of Oceanyx Pharmaceuticals, Inc., which has licensed patents and patent applications related to the subject matter.

model that closely mimics the human pancreatic tumor microenvironment was for the first time used in apratoxin studies. Apra S10 showed promising antitumor effect in this pancreatic cancer model and this effect was mediated through anti-proliferation effects.

Keywords

pancreatic adenocarcinoma; cotranslational translocation; secretory pathway; drug resistance

Introduction

Pancreatic cancer (PC) is associated with a dismal 5-year survival (8%) and it is projected to surpass colorectal cancer to become the second leading cause of cancer-related deaths in the United States by 2030. [1, 2] The current standard pancreatic cancer treatment is chemotherapy with or without radiation, which provides minimal survival benefit. The first-line therapy, gemcitabine or FOLFIRINOX treatment, only increased patients' survival by a few months.[3] The combination therapy of gemicitabine and a targeted therapeutic agent, erlotinib, although approved by FDA, was not widely used on patients due to limited clinical utility and intolerable toxicity.[4] One explanation for the poor therapeutic outcome in PC is the desmoplastic response in the tumor microenvironment which does not allow for therapeutic penetration. The tumor microenvironment is characterized by altered extracellular matrix production, poor vasculatures, and hyper-active fibroblasts.[5, 6] This strong stromal component found throughout the PC tumor microenvironment may serve as a mechanical barrier for PC evasion of the immune response and diminished anticancer drug delivery and efficacy.[7, 8] Efforts have been made to overcome this barrier by enhancing drug delivery or increasing intratumoral drug concentration. Examples include targeting non-tumor components within the desmoplastic tumor microenvironment,[7] increasing local drug concentrations in pancreas through intra-arterial chemotherapy,[9, 10] and targeted drug delivery (e.g. albumin-bound (nab)-paclitaxel and nanotechnology-based drug delivery).[11–13] In addition to drug delivery enhancement, other efforts are focusing on altering the tissue distribution pattern of small molecule anticancer agents by structural modifications, aimed at improving their distribution in the pancreas.[14] For example, a difluoro-analogue of curcumin has enhanced bioavailability and pancreatic enrichment than the parent compound.[14] Another possible explanation for the unfavorable clinical response of pancreatic cancer therapies is due to the intrinsic resistance of pancreatic cancer cells, driven by abnormal signaling pathways as well as secretion of soluble growth factors from the stroma that stimulate pancreatic cancer growth.[5, 15] Given the challenges and the rising incidence of PC, there is an urgent necessity to develop novel therapeutic strategies to enhance local drug concentration and increase drug efficacy.

Apratoxins are a family of potent anticancer and antiangiogenic agents which significantly retarded tumor growth in a HCT116 (human colon cancer) subcutaneous tumor mouse model.[16–20] The potent activity of apratoxins is associated with their ability to downregulate both receptor tyrosine kinases (RTKs) and their ligands including vascular endothelial growth factor A (VEGF-A) and interleukin 6 (IL-6), mediated through blocking one stage of secretory pathways, cotranslational translocation, at the level of Sec61.[18, 20–

22]. This unusual mechanism of action of apratoxins suggested their potential therapeutic use against cancers with active secretive pathways such as pancreatic cancer. The pancreas is a major secretory organ and the majority of pancreatic exocrine tumors are adenocarcinomas that arise from ductal epithelium.[23, 24] We hypothesized that apratoxins possess high affinity to pancreatic tissue due to the fact that the secretory machinery in pancreas is the natural target of apratoxins.

We recently reported the design, synthesis and in vitro characterization of a novel apratoxin analogue, apratoxin S10 (Apra S10) as a potential therapeutic antitumor agent (Fig. 1). [20] Compared with other apratoxins, Apra S10 is superior in achieving a balance of stability, potency and synthetic yield.[20] To evaluate its efficacy as a pancreatic cancer agent, it is crucial to apply an effective tumor model system which mimics the unique tumor microenvironment. To overcome this major obstacle, we used an orthotopic pancreatic patient-derived xenografts (PDX) model that preserves the stromal component of native pancreatic tumor, results in frequent clinically similar metastases, and induces muscle wasting characteristic of the cancer cachexia syndrome.[25] The orthotopic model also better recapitulates the human disease as compared to a flank model because the tumor becomes part of the portal venous system. This is an important concept because the active secretory profile of tumor will have a first pass flow through the liver rather than the lungs creating signaling pathways that mimics the human disease in a way that the flank model does not recapitulate. Our studies using several in vitro and in vivo models indicated that Apra S10 exerts promising efficacies to combat pancreatic cancer.

Methods

Cell culture

Primary patient derived pancreatic cancer cell lines EC46 and EC68, isolated as previously described[26] and PANC-1 cells were cultured in DMEM/F-12K (1:1 mixture) medium supplemented with 10% fetal bovine serum. Tumor associated stromal cells TAS-G13, isolated as previously described[27] were also cultured in DMEM/F-12K media. All cells were maintained at 37 ºC humidified air and 5% CO_2.

Cell Viability Assay (MTT)

PANC-1, EC46 or EC68 cells were seeded in a 96-well clear bottom plate at cell densities of 5000 cells per well. Cells were allowed to attach overnight, followed by treatment with various concentrations of the Apra S10, erlotinib or solvent control (EtOH). After 48 h of incubation, cell viability was measured using MTT according to the manufacturer's instructions (Promega, Madison, WI). Nonlinear regression analysis was carried out using GraphPad Prism software for GI_{50} and IC_{50} value calculations.

Total synthesis of Apra S10

Apra S10 was synthesized as previously described.[20]

Immunoblot analysis

PANC-1 and EC46 cells were seeded at 200,000/well in 6-well clear bottom plates and allowed to attach overnight. Cells were treated with Apra S10 or solvent control (EtOH) after replacing with fresh media. Whole cell lysates were collected 24 h post treatment using PhosphoSafe buffer (EMD Chemicals, Inc, Gibbstown, NJ). Protein concentrations were measured with the BCA Protein Assay kit (Thermo Fisher Scientific, Rockford, IL). Lysates containing equal amounts of protein were separated by SDS polyacrylamide gel electrophoresis (4–12%), transferred to polyvinylidene difluoride membranes, probed with primary and secondary antibodies, and detected with the SuperSignal West Femto Maximum Sensitivity Substrate (Thermo Fisher Scientific). Anti-EGFR, Met, IGF-1Rβ, β-actin and secondary anti-mouse and rabbit antibodies were from Cell Signaling Technology, Inc (Danvers, MA).

VEGF-A AlphaLISA

PANC-1 (5000 cells/well) and EC46 (10,000 cells/well) were seeded in a 96-well clear bottom plate and allowed to attach overnight. Cells were treated with various concentrations of Apra S10 or solvent control (EtOH) after replacing with fresh media. Culture supernatants were collected after 12 h incubation for detection of VEGF-A using AlphaLISA kit (PerkinElmer, Waltham, MA) following the manufacturer's instruction. Briefly, acceptor bead and anti-VEGF-A antibody were incubated with the supernatants for 60 min followed by incubation with donor beads for an additional 30 min. Signal was detected using Envision (PerkinElmer) and VEGF-A secretion levels are reported relative to solvent control with normalization to cell viability at 12 h measured by MTT assay.

Partial secretome profiling

EC68 (5000 cells/well) and TAS-G13 (5000 cells/well) were seeded in 96-well clear bottom plates and allowed to attach overnight. Medium was replaced with serum free media and cells were allowed to grow an additional 24 h following which cells were treated in triplicate with Apra S10 (10 nM, 1 nM and 100 pM) and EtOH control. Culture supernatants from triplicate wells for each concentration were combined following 12 h incubation with drug or solvent. Supernatants were stored at −20 °C until Luminex assay was performed using EMD MILLIPLEX® human cytokine/chemokine magnetic bead panel assay kit (EMD Millipore, Billerica, MA) following manufacturers protocol. Assay was carried out in triplicate, validated using quality control samples provided in the kit and cytokine levels measured using a standard curve for human cytokine provided in the kit. Data was analyzed using Milliplex Analyst software and shown as % secretion relative to solvent control.

Tissue distribution and plasma and tissue collection

Four- to ten- week old NOD-SCID IL2 receptor gamma chain knockout (NSG) female mice from Jackson Laboratory (Bar Harbor, ME) were randomly distributed into two administration groups: 1 mg/kg Apra S10 treatment group (36 mice) and sham group (4 mice). Mice in treatment group were further randomly assigned into twelve administration subgroups (3 mice per group): sacrificed at six different time points following i.v. or i.p. administration. Apra S10 was formulated in 10% EtOH, 5% Tween-80, 85% saline solution

(100 μL/20 g mice) for i.v. injection and formulated in DMSO (25 μL/20 g mice) for i.p. injection.

Pancreas, liver, lung, salivary glands, spleen, kidney, brain and whole blood were collected at 10 minutes, 1, 3, 8, 24, and 48 hours after a single i.v. or i.p. administration of 1 mg/kg Apra S10. Blood samples were centrifuged at 15,000 *g* for 90 seconds to collect the plasma. Plasma and tissue samples were snap frozen in liquid nitrogen and stored at −80 °C until analysis.

Sample preparation

Tissues were thawed on ice and three volumes of PBS buffer was added. Tissues were homogenized on ice and centrifuged for 5 min (16,000 *g*, 4 °C) to collect tissue homogenates. Plasma or tissue homogenates (50 μL) were transferred into Eppendorf tubes followed by addition of 150 μL of 0.067 μg/mL harmine in 1:1 acetonitrile/methanol into each. Each ample was mixed and centrifuged at 10,000 *g* for 5 min at 4 °C. The supernatant was collected and evaporated to dryness under nitrogen. Compounds were reconstituted with 50 μL of acetonitrile and the obtained solution was filtered through nylon membrane containing centrifuge tubes (Corning) and subjected to LC-MS/MS analysis.

LC-MS/MS analysis

A volume of 10 μL of the reconstituted solution was injected into the LC-MS system. LC-MS was done on a 3200 QTRAP (Applied Biosystems) equipped with a Shimadzu (Kyoto, Japan) UFLC System [column, Onyx Monolithic C18 (3.0 × 100 mm), Phenomenex (Torrance, CA); solvent, water (solvent A) acetonitrile (solvent B); flow rate, 0.5 mL/min; detection by electrospray ionization (ESI)-MS in positive ion mode using multiple reaction monitoring (MRM) scan)]. A stepwise gradient elution was used starting at 50% B, then increasing to 60% B at 2 min and maintained at this condition for 6 min, then further increasing to 80% B in 5 min. MS parameters were optimized before analysis by using direct syringe infusion. The retention times (t_R, min; MRM ion pair) of the analytes and internal standard were as follows: harmine (3.11; 213.1→ 170.1), Apra S10 (11.4; 842.5→ 446.1). Compound-dependent parameters used were as follows: Apra S10, declustering potential (DP) 51 V, entrance potential (EP) 12 V, collision energy (CE) 41 V, collision cell exit potential (CXP) 22 V, collision cell entrance potential (CEP) 36 V; and harmine, DP 46 V, EP 4 V, CE 35 V, CXP 4 V, CEP 15 V. Source gas parameters used were as follows: curtain gas, 15 psi; collision gas low, ion spray voltage 4200 V; temperature, 600 °C; ion source gas 1, 50 psi; ion source gas 2, 60 psi.

Calibration curves for Apra S10 in each biological matrix were generated by least-square linear regression analysis of the analyte peak area and internal standard peak area ratio against the nominal concentration of the standard solutions. All calculations were done using Analyst 1.6.2 software (Applied Biosystems) in Quantitate Mode.

PK parameter analysis

Apra S10 concentration-time data were fitted using noncompartmental analysis in Phoenix™ 64 WinNonlin® (Pharsight, Certara). PK parameters including elimination rate

constant (k_e), half-life ($t_{1/2}$), peak concentration (C_{max}), time to peak concentration (T_{max}), area under the concentration-time curve (AUC_t), area under the concentration-time curve to infinity (AUC), clearance (CL/F), volume of distribution (V_z/F), and mean residence time (MRT) were estimated and listed in Table 2. Linear trapezoidal rule was used for AUC_t calculation, AUC infinity was extrapolated as the sum of AUC_t and the last quantifiable concentration (C_{last}) divided by terminal slope on log scale (λ_z). CL was computed as dose divide by AUC and MRT was calculated as the area under the first moment curve (AUMC) divide by AUC. Tissue to plasma partition coefficients (K_p) were calculated using tissue concentrations divided by average plasma concentration at the corresponding time point.

Simulation study

Simulation was also conducted in Phoenix where 0.25 mg/kg Apra S10 was administered i.p. with dosing intervals of 24 hours and 48 hours respectively. Simulation of two dosing interval of Apra S10 was derived from single dose PK experiment. The predicted concentration-time profiles are shown in Fig. 4. The dashed horizontal line (red) indicates a concentration of 40 ng/mL Apra S10, the minimum effective concentration. Steady state pancreas concentration is expected to achieve after four doses of Apra S10 if it is dosed every day or after two doses of Apra S10 if it is dosed every other day.

In vivo efficacy study of Apra S10 in orthotopic PDX mouse model

The PDX model was established as previously described. [25, 28] In brief, a human PC specimen was collected at the time of operation from a patient with surgically resected pancreatic ductal adenocarcinoma as verified by pathology, cut into 3 × 3mm cubes, and then implanted into the right flank of female NSG mice. PDXs were grown to 2.0 cm before passage into next generation of mice to allow for expansion of tumor for future studies.

NSG mice were orthotopically implanted with the second generation PDX tumor. Mice were then randomized into vehicle and Apra S10 treatment groups at post-operative day 45 when the tumors reached palpable sizes, a diameter of 3–4 mm. Mice were injected intraperitoneally (i.p.) with 0.25 mg/kg Apra S10 or DMSO control every other day until the endpoint. Tumor dimensions were measured using calipers every three to five days and tumor volumes were calculated using the formula II $(D\text{-}1)^3/6$, where diameter (D) is the average diameter calculated using calipers and the LOGIQ e Vet model ultrasound (General Electric, Fairfield, CT).

Organs were procured at endpoint, tumor tissue was placed in formalin and then embedded in paraffin. Subsequently, 5 micron paraffin sections were obtained and underwent TUNEL staining for apoptosis and Ki-67 staining for proliferation. All studies were carried out under the protocol approved by the Institutional Animal Care and Use Committee (IACUC) at the University of Florida.

Results

Apra S10 inhibits proliferation of both established and primary pancreatic cancer cells at low nanomolar concentrations

To evaluate Apra S10's activity in pancreatic cancer, we first obtained established pancreatic cancer cells, PANC-1(*KRAS*, G12D; *TP53*, 273H)[29], which are frequently used as in vitro models for studies of exocrine pancreatic cancer. Apra S10 potently inhibited the proliferation of PANC-1 at low nanomolar GI_{50} range, while the FDA approved EGFR inhibitor for pancreatic cancer treatment, erlotinib, showed thousands fold less activity (Table 1). PANC-1 cells have been passaged and cultured in vitro in a two-dimensional monolayer for several decades, which can lead to genetic mutations and morphological changes and may not accurately represent pancreatic cancer.[29, 30] The disconnection between preclinical results and clinical outcomes may be in part due to the poor representation of this disease in preclinical models. PC is a heterogeneous disease with different genetic variations leading to different phenotypes within the disease. The Trevino group has established a method to expand primary human pancreatic cancer cell lines from a PDX mouse model which allowed us to test Apra S10 on adenocarcinoma cells, that have not been cultured in vitro on a plastic surface for years, to more closely mimic native cancer cells.[26] Apra S10 was tested on two of these primary pancreatic cell lines EC46 (*KRAS*, G12V; *TP53*, WT) and EC68 (*KRAS*, G12D; *TP53*, R248W). The growth of both EC46 and EC68 cells were inhibited by Apra S10 with GI_{50}s of 0.32 and 0.35 nM, respectively (Table 1). In contrast, erlotinib only showed activity in the micromolar range (Table 1).

Apra S10 potently downregulated various RTKs and inhibited the secretion of VEGF-A at low nanomolar to subnanomolar concentrations (Fig. 2a, b). We subsequently profiled 41 secreted factors to establish a substrate selectivity profile in primary PC cells (EC68) as well as tumor associated stromal cells (TAS-G13). The results suggested that not all factors are inhibited to equal extent and several are unchanged or possibly increased (Fig. 2c–e), arguing against nonselective cytotoxicity without substrate specificity supposedly displayed by apratoxin A.[22] Since stromal cells secret factors that stimulate pancreatic cancer cell growth,[15] our finding that Apra S10 inhibits their secretion is considered as one potential mechanism by which Apra S10 could overcome drug resistance.

Tissue distribution study demonstrated high enrichment of Apra S10 in the pancreas

With the encouraging results of Apra S10's activity against pancreatic cancer in vitro, we then aimed to investigate whether Apra S10 has high distribution in the pancreas. We performed a tissue distribution and pharmacokinetic study of Apra S10 in NSG mice. Both intraperitoneal (i.p.) and intravenous (i.v.) injection routes were performed, considering both routes have been used in previous apratoxins in vivo studies.[19, 31, 32] Tissues and plasma were collected at six time points following a single i.v. or i.p. administration of Apra S10 at 1 mg/kg. Concentrations of Apra S10 in tissues and plasma were quantified using liquid chromatography tandem mass spectrometry (LCMS/MS). Pancreas has the highest peak concentrations of Apra S10 in both administration routes, followed by salivary glands, spleen, liver, lung, kidney and brain (Fig. 3a). The non-compartmental pharmacokinetic analysis was utilized to obtain the steady-state pharmacokinetic parameters of each

individual's concentration-time profile (Table 2). The tissue: plasma partition coefficients (*K*p), a good indicator of the extent of tissue distribution, was calculated to determine pancreas as the major distribution organ (Fig. 3b, c). Both i.p. and i.v. administration have similar distribution profiles across organs and similar time course concentrations in each organ as seen in Fig. 3, meaning that regardless of the route given, the drug will accumulate in the pancreas. This also allows us to compare our results to other studies using either administration route.

Apra S10 had significant anti-tumor effect in a pancreatic patient-derived xenograft (PDX) mouse model

After confirming that Apra S10 has a favorable tissue distribution in pancreas, we were prompted to test its efficacy in a pancreatic PDX model. A simulation study was first conducted to identify an appropriate in vivo dose and a dosing schedule of Apra S10 aimed at achieving an effective intratumoral concentration in pancreatic cancer. The in vitro studies suggested the concentrations of Apra S10 required to achieve the maximal response are around 50 nM (40 ng/mL) (Fig. 1). Simulation results demonstrated that, in order to achieve a stabilized concentration above 40 ng/mL in pancreas over time, every-other-day dosing with Apra S10 at 0.25 mg/kg is sufficient (Fig. 4). We next evaluated Apra S10 in a PDX mouse model using the optimized dose and dosing schedule above. Apra S10 significantly retarded tumor growth in this PDX mouse model (Fig. 5a; Fig. 6) without causing weight loss (Fig. 5b).

Apra S10 reduced proliferation of PDX tumors in vivo

To determine the mechanism by which Apra S10 was decreasing the tumor growth, we measured both proliferation and apoptosis. Staining of the tumors for Ki-67, a marker of cellular proliferation, showed a significant difference between vehicle and Apra S10 treated mice (Fig. 7). Apra S10 caused more than a 50% decrease in the number of cells undergoing proliferation at the time of euthanasia. Using a TUNEL stain to detect apoptotic cells, no difference was found between Apra S10 and vehicle groups in the number of cells undergoing apoptosis at the time of euthanasia (Fig. 7).

Discussion

Apratoxins are potent cytotoxic agents derived from marine cyanobacteria.[16, 32–36] Apratoxin A was the first compound discovered in apratoxin family which possesses broad-spectrum differential in vitro activities.[17] Its cytotoxicity is due to potent inhibition of cotranslational translocation[21] at the level of the Sec61 translocon,[22, 31] leading to both downregulation of various receptor tyrosine kinases and reduced growth factor secretion.[21] Although apratoxin A showed potent antitumor activities in vivo, it caused intolerable toxicity which limited its therapeutic use.[16, 31] The toxicity of apratoxin A is possibly associated with its accumulation in normal pancreas which lead to pancreas atrophy.[31] In order to improving therapeutic index of apratoxin A, our group has spent considerable efforts on a medicinal chemistry campaign, which led to apratoxins S4, S8–10, possessing potent in vitro as well as in vivo anticancer activities and enhanced in vitro stability.[18–20] Apratoxins S4 and S8 were evaluated in a colon cancer xenograft mice model and both

analogues significantly retarded tumor growth at 0.25 mg/kg of daily dosing.[18, 19] Apra S10 is the newest analogue we discovered, which is considered one of the lead candidates of the apratoxin family in terms of potency, stability, and synthetic accessibility. [20]

Here, we have characterized Apra S10 as a novel drug for the treatment of pancreatic cancer in preclinical models. Growth of both established pancreatic cancer cell line and new primary pancreatic cancer cell lines was effectively inhibited by Apra S10 at nano- to sub-nanomolar concentrations, suggesting Apra S10's therapeutic effectiveness across the genetic heterogeneity seen in PC. Tissue distribution data demonstrated that Apra S10 reaches the highest concentrations in the pancreas across the time points with only the salivary gland concentrations coming close to the pancreas drug concentrations. Thus, our data support that apratoxins distribute to organs with exocrine function which is consistent with their mechanism of action of secretory pathway inhibition and Sec61 blockage.[21, 22, 31] The pancreatic enrichment is ideal for obtaining therapeutic intratumoral concentrations while maintaining lower concentrations in other organs reducing the toxic side effects of the drug, making it an ideal drug to target diseases of the pancreas. Due to the high bioavailability and half-life in the pancreas, dosing with 0.25 mg/kg every other day (instead of daily) was sufficient to maintain an effective local concentration, potentially further reducing undesirable side effects. To our knowledge, this is the first study of apratoxins in an orthotopic PDX model which allowed us to test apratoxins in a more natural environment. Using a PDX model does require the use of immunodeficient mice such as the NSG mice used in these experiments. Although this model lacks an adaptive immune system, it has an intact innate immune system which maintains important immune signaling profiles from the tumor. In the orthotopic PDX preclinical model, Apra S10 inhibited tumor growth and the effect was associated with reduced cellular proliferation in the tumor. We have not yet elucidated the exact mechanism by which Apra S10 is causing this inhibition in proliferation rather than an increase in apoptosis, but we speculate the decrease in proliferation may be the result of the protective microenvironment in the orthotopic PDX model or that apoptosis would require higher Apra S10 concentrations, indicating that the cytotoxic and cell growth effects can be separated. In conclusion, our findings suggest Apra S10 could be a useful adjunct to current cytotoxic therapies for pancreatic cancer.

Acknowledgments

Funding

Research was supported in part by the National Institutes of Health, NCI grant R01CA172310, Ocala Royal Dames for Cancer Research, Inc., NCI Research Specialist Award R50CA211487 (R.R) and the Debbie and Sylvia DeSantis Chair professorship (H.L.).

References

1. Siegel RL, Miller KD, Jemal A (2016) Cancer statistics. CA Cancer J Clin 66:7–30 [PubMed: 26742998]
2. Rahib L, Smith BD, Aizenberg R, Rosenzweig AB, Fleshman JM, Matrisian LM (2014) Projecting cancer incidence and deaths to 2030: The unexpected burden of thyroid, liver, and pancreas cancers in the united states. Cancer Res. 74:2913–2921 [PubMed: 24840647]
3. Conroy T, Desseigne F, Ychou M, Bouché O, Guimbaud R, Bécouarn Y, Adenis A, Raoul J-L, Gourgou-Bourgade S, de la Fouchardière C, Bennouna J, Bachet J-B, Khemissa-Akouz F, Péré-

Vergé D, Delbaldo C, Assenat E, Chauffert B, Michel P, Montoto-Grillot C, Ducreux M (2011) FOLFIRINOX versus gemcitabine for metastatic pancreatic cancer. N Engl J Med 364:1817–1825 [PubMed: 21561347]

4. Moore MJ, Goldstein D, Hamm J, Figer A, Hecht JR, Gallinger S, Au HJ, Murawa P, Walde D, Wolff RA, Campos D, Lim R, Ding K, Clark G, Voskoglou-Nomikos T, Ptasynski M, Parulekar W (2007) Erlotinib plus gemcitabine compared with gemcitabine alone in patients with advanced pancreatic cancer: A phase III trial of the National Cancer Institute of Canada Clinical Trials Group. J Clin Oncol 25:1960–1966 [PubMed: 17452677]
5. Long J, Zhang Y, Yu X, Yang J, LeBrun DG, Chen C, Yao Q, Li M (2011) Overcoming drug resistance in pancreatic cancer. Expert Opin Ther Targets 15:817–28 [PubMed: 21391891]
6. Chiaravalli M, Reni M, O'Reilly EM (2017) Pancreatic ductal adenocarcinoma: State-of-the-art 2017 and new therapeutic strategies. Cancer Treat. Rev 60:32–43 [PubMed: 28869888]
7. Yu M, Tannock IF (2012) Targeting tumor architecture to favor drug penetration: A new weapon to combat chemoresistance in pancreatic cancer? Cancer Cell 21:327–329 [PubMed: 22439929]
8. Whatcott C, Han H, Posner RG, Von Hoff DD (2013) Tumor-stromal interactions in pancreatic cancer. Crit Rev Oncog 18:135–151 [PubMed: 23237556]
9. Jin C, Yao L, Long J, Fu D, Yu X, Xu J, Yang F, Ni Q (2009) Effect of multiple-phase regional intra-arterial infusion chemotherapy on patients with resectable pancreatic head adenocarcinoma. Chin Med J (Engl) 122:284–290 [PubMed: 19236805]
10. Liu F, Tang Y, Sun J, Yuan Z, Li S, Sheng J, Ren H, Hao J (2012) Regional intra-arterial vs. systemic chemotherapy for advanced pancreatic cancer: A systematic review and meta-analysis of randomized controlled trials. PLoS One 7:e40847 [PubMed: 22815840]
11. Von Hoff DD, Ramanathan RK, Borad MJ, Laheru DA, Smith LS, Wood TE, Korn RL, Desai N, Trieu V, Iglesias JL, Zhang H, Soon-Shiong P, Shi T, Rajeshkumar NV., Maitra A, Hidalgo M (2011) Gemcitabine plus nab-paclitaxel is an active regimen in patients with advanced pancreatic cancer: A phase I/II trial. J Clin Oncol 29:4548–4554 [PubMed: 21969517]
12. Frese KK, Neesse A, Cook N, Bapiro TE, Lolkema MP, Jodrell DI, Tuveson DA (2012) Nab-paclitaxel potentiates gemcitabine activity by reducing cytidine deaminase levels in a mouse model of pancreatic cancer. Cancer Discov 2:260–269 [PubMed: 22585996]
13. Yang F, Jin C, Jiang Y, Li J, Di Y, Ni Q, Fu D (2011) Liposome based delivery systems in pancreatic cancer treatment: From bench to bedside. Cancer Treat Rev 37:633–642 [PubMed: 21330062]
14. Padhye S, Banerjee S, Chavan D, Pandye S, Swamy KV, Ali S, Li J, Dou QP, Sarkar FH (2009) Fluorocurcumins as cyclooxygenase-2 inhibitor: Molecular docking, pharmacokinetics and tissue distribution in mice. Pharm Res 26:2438–2445 [PubMed: 19714451]
15. Straussman R, Morikawa T, Shee K, Barzily-Rokni M, Qian ZR, Du J, Davis A, Mongare MM, Gould J, Frederick DT, Cooper ZA, Chapman PB, Solit DB, Ribas A, Lo RS, Flaherty KT, Ogino S, Wargo JA, Golub TR (2012) Tumour micro-environment elicits innate resistance to RAF inhibitors through HGF secretion. Nature 487:500–504 [PubMed: 22763439]
16. Luesch H, Yoshida WY, Moore RE, Paul VJ, Corbett TH (2001) Total structure determination of apratoxin A, a potent novel cytotoxin from the marine cyanobacterium Lyngbya majuscula. J Am Chem Soc 123:5418–5423 [PubMed: 11389621]
17. Luesch H, Chanda SK, Raya RM, DeJesus PD, Orth AP, Walker JR, Izpisúa Belmonte JC, Schultz PG (2006) A functional genomics approach to the mode of action of apratoxin A. Nat Chem Biol 2:158–167 [PubMed: 16474387]
18. Chen QY, Liu Y, Luesch H (2011) Systematic chemical mutagenesis identifies a potent novel apratoxin A/E hybrid with improved in vivo antitumor activity. ACS Med Chem Lett 2:861–865 [PubMed: 22081789]
19. Chen QY, Liu Y, Cai W, Luesch H (2014) Improved total synthesis and biological evaluation of potent apratoxin S4 based anticancer agents with differential stability and further enhanced activity. J Med Chem 57:3011–3029 [PubMed: 24660812]
20. Cai W, Chen Q-Y, Dang LH, Luesch H (2017) Apratoxin S10, a dual inhibitor of angiogenesis and cancer cell growth to treat highly vascularized tumors. ACS Med Chem Lett 8:1007–1012 [PubMed: 29057042]

21. Liu Y, Law BK, Luesch H (2009) Apratoxin A reversibly inhibits the secretory pathway by preventing cotranslational translocation. Mol Pharmacol 76:91–104 [PubMed: 19403701]
22. Paatero AO, Kellosalo J, Dunyak BM, Almaliti J, Gestwicki JE, Gerwick WH, Taunton J, Paavilainen VO (2016) Apratoxin kills cells by direct blockade of the Sec61 protein translocation channel. Cell Chem Biol 23:561–566 [PubMed: 27203376]
23. Singh D, Upadhyay G, Srivastava RK, Shankar S (2015) Recent advances in pancreatic cancer: biology, treatment, and prevention. Biochim Biophys Acta -Rev Cancer 1856:13–27
24. Chandra R, Liddle RA (2009) Neural and hormonal regulation of pancreatic secretion. Curr Opin Gastroenterol 25:441–446 [PubMed: 19535978]
25. Go KL, Delitto D, Judge SM, Gerber MH, George TJ, Behrns KE, Hughes SJ, Judge AR, Trevino JG (2017) Orthotopic Patient-Derived Pancreatic Cancer xenografts engraft into the pancreatic parenchyma, metastasize, and induce muscle wasting to recapitulate the human disease. Pancreas 46:813–819 [PubMed: 28609371]
26. Pham K, Delitto D, Knowlton AE, Hartlage ER, Madhavan R, Gonzalo DH, Thomas RM, Behrns KE, George TJ, Hughes SJ, Wallet SM, Liu C, Trevino JG (2016) Isolation of pancreatic cancer cells from a patient-derived xenograft model allows for practical expansion and preserved heterogeneity in culture. Am J Pathol 186:1537–1546 [PubMed: 27102771]
27. Han S, Delitto D, Zhang D, Sorenson HL, Sarosi GA, Thomas RM, Behrns KE, Wallet SM, Trevino JG, Hughes SJ (2015) Primary outgrowth cultures are a reliable source of human pancreatic stellate cells. Lab Investig 95:1331–1340 [PubMed: 26322418]
28. Delitto D, Pham K, Vlada AC, Sarosi GA, Thomas RM, Behrns KE, Liu C, Hughes SJ, Wallet SM, Trevino JG (2015) Patient-derived xenograft models for pancreatic adenocarcinoma demonstrate retention of tumor morphology through incorporation of murine stromal elements. Am J Pathol 185:1297–1303 [PubMed: 25770474]
29. Rückert F, Aust D, Böhme I, Werner K, Brandt A, Diamandis EP, Krautz C, Hering S, Saeger HD, Grützmann R, Pilarsky C (2012) Five primary human pancreatic adenocarcinoma cell lines established by the outgrowth method. J Surg Res 172:29–39 [PubMed: 21683373]
30. Lieber M, Mazzetta J, Nelson- Rees W, Kaplan M, Todaro G (1975) Establishment of a continuous tumor- cell line (PANC- 1) from a human carcinoma of the exocrine pancreas. Int J Cancer 15:741–747 [PubMed: 1140870]
31. Huang K-C, Chen Z, Jiang Y, Akare S, Kolber-Simonds D, Condon K, Agoulnik S, Tendyke K, Shen Y,Wu K-M, Mathieu S, Choi H -w., Zhu X, Shimizu H, Kotake Y, Gerwick WH, Uenaka T, Woodall-Jappe M, Nomoto K (2016) Apratoxin A shows novel pancreas-targeting activity through the binding of Sec61. Mol Cancer Ther 15:1208–1216 [PubMed: 27196783]
32. Tidgewell K, Engene N, Byrum T, Media J, Doi T, Valeriote FA, Gerwick WH (2010) Evolved diversification of a modular natural product pathway: Apratoxins F and G, two cytotoxic cyclic depsipeptides from a Palmyra collection of *Lyngbya bouillonii*. ChemBioChem 11:1458–1466 [PubMed: 20512792]
33. Luesch H, Yoshida WY, Moore RE, Paul VJ (2002) New apratoxins of marine cyanobacterial origin from Guam and Palau. Bioorganic Med Chem 10:1973–1978
34. Gutiérrez M, Suyama TL, Engene N, Wingerd JS, Matainaho T, Gerwick WH (2008) Apratoxin D, a potent cytotoxic cyclodepsipeptide from papua new Guinea collections of the marine cyanobacteria *Lyngbya majuscula* and *Lyngbya sordida*. J Nat Prod 71:1099–1103 [PubMed: 18444683]
35. Matthew S, Schupp PJ, Luesch H (2008) Apratoxin E, a cytotoxic peptolide from a guamanian collection of the marine cyanobacterium *Lyngbya bouillonii*. J Nat Prod 71:1113–1116 [PubMed: 18461997]
36. Thornburg CC, Cowley ES, Sikorska J, Shaala LA, Ishmael JE, Youssef DTA, McPhail KL (2013) Apratoxin H and apratoxin A sulfoxide from the red sea cyanobacterium *Moorea producens*. J Nat Prod 76:1781–1788 [PubMed: 24016099]

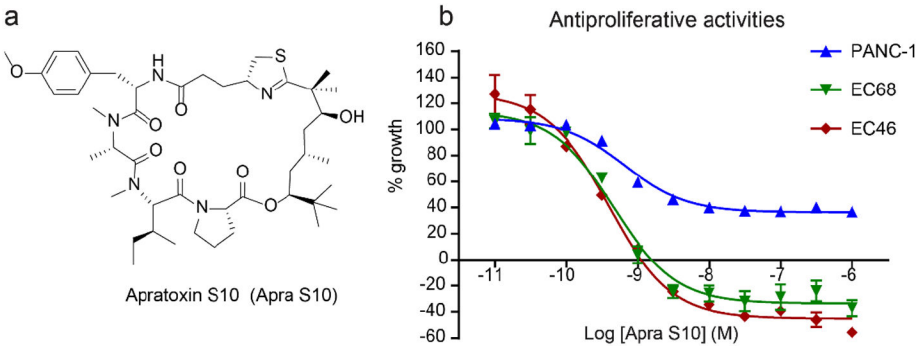

Fig. 1.

Structure of Apra S10 (a) and the effects of Apra S10 on cell growth of EC68, EC46 (primary pancreatic cancer cells) and PANC-1 (exocrine pancreatic cancer cells) using an MTT assay at 48 hours (b).

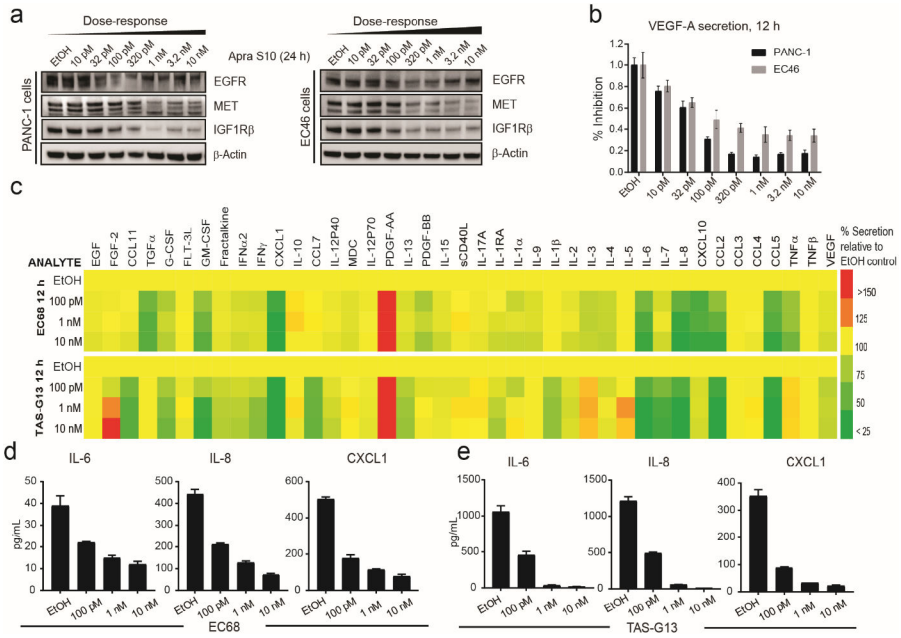

Fig. 2.

In vitro activity of Apra S10 in PC cells and tumor associated stromal (TAS-G13) cells. Effects on (a) RTKs (24 h) and (b) VEGF-A secretion (12 h) in PANC-1 and EC46 cells. (c) Effects of on secretion of 41 cytokines/ growth factors in primary cancer EC68 cells (top), tumor associated stromal TAS-G13 cells (bottom). Several affected factors are displayed in (d) for PC and (e) for stromal cells (average of triplicates).

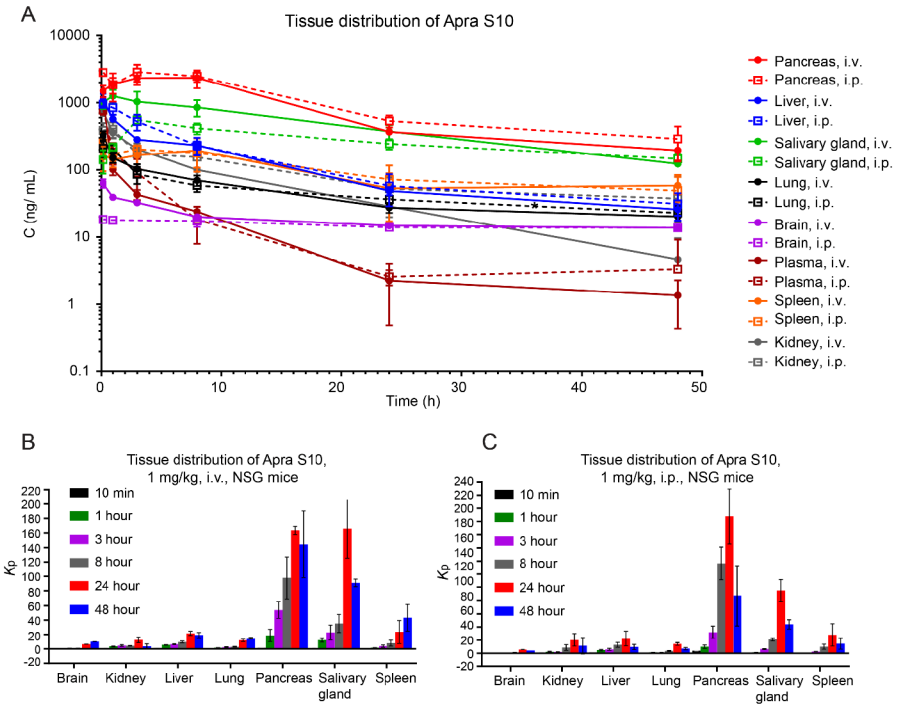

Fig. 3.

Concentrations of Apra S10 in plasma and tissues following a single i.v. or i.p. administration of 1 mg/kg Apra S10 to mice (a). Solid lines indicate i.v. tissue distribution profiles. Dashed lines indicate i.p. profiles. Numbers represent the average of three mice in each group, with error bars indicating SD. Tissue distribution histogram of i.v. (b) and i.p. (c) administration. K_p: tissue:plasma partition coefficients. Numbers represent the average of three mice in each group, with error bars indicating SD.

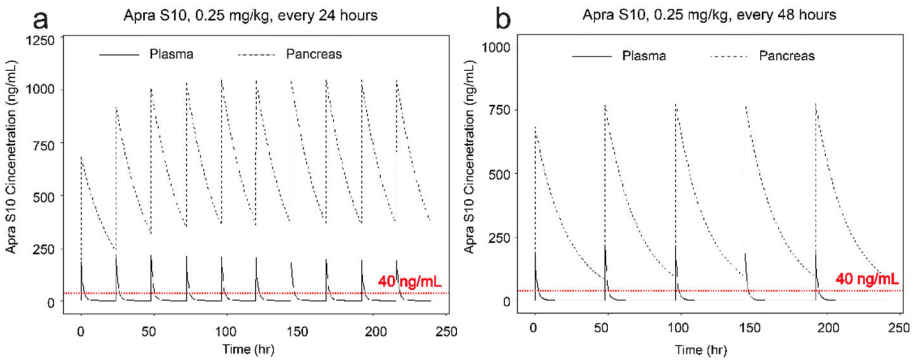

Fig. 4.

Simulation for Apra S10 doses to achieve a concentration above 40 ng/mL. The dosing intervals considered were (a) daily, (b) every other day. The dashed horizontal lines (red) represent the minimum effective concentration, 40 ng/mL.

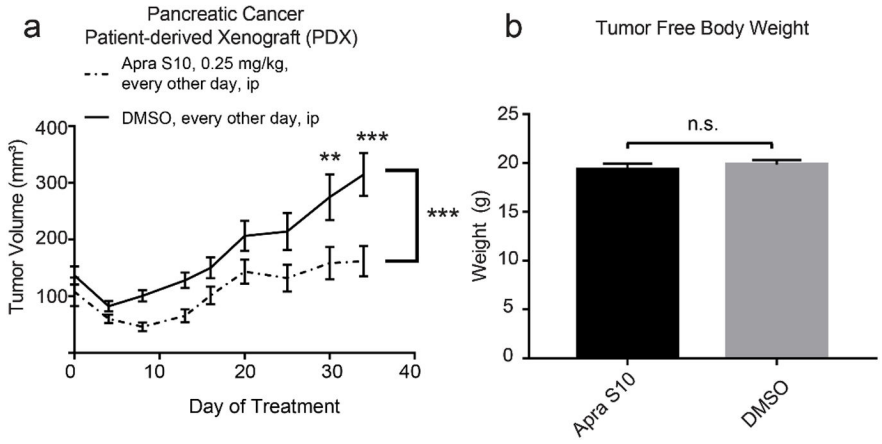

Fig. 5.

(a) Tumor volume over the course of treatment, plotted as mean with standard error. P-values were calculated using a repeated measures two-way ANOVA and Sidak's multiple comparisons test for each individual time points. (b) tumor free body weight upon euthanasia of mice. P-values were calculated using a student's t-test and plotted as mean with standard error. *P < 0.05, **P < 0.01, ***P < 0.001.

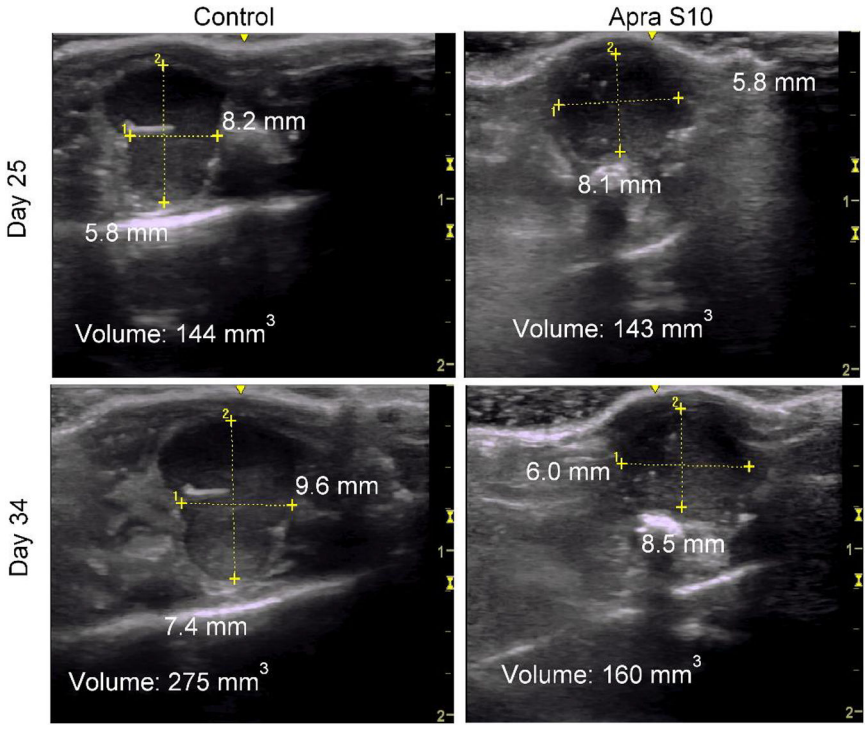

Fig. 6.

Ultrasound images of a representative control DMSO treated mouse on the left with area and volume at Day 25 (top left) and Day 34 (bottom left) as shown. Representative ultrasound images of an Apra S10 treated mouse on the right with area and volume at Day 25 (top right) and Day 34 (bottom right) as shown. Scale in centimeters on right side of each ultrasound image.

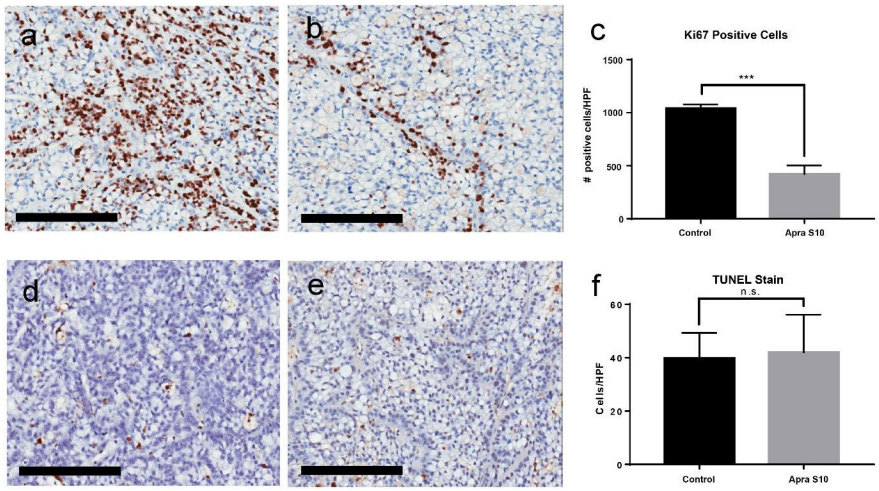

Fig. 7.

Representative images of tumors stained for Ki-67 *brown* of (a) control mouse and (b) Apra S10 treated mouse. (d) The average number of positive cells per HPF calculated using ImageJ. Representative images of tumors with TUNEL staining *brown* of (d) control mouse and (e) Apra S10 treated mouse. (f) The average number of positive cells per HPF by manual calculation. Scale bars represent 200 μm. Error bars represent SD. *HPF* High powered field; *** P-value < 0.001

Table 1.

GI50 (nM) of Apra S10 and IC50 (nM) of a clinically approved receptor tyrosine kinase (EGFR) inhibitor on both established and new patient derived pancreatic cancer cell lines

Compounds	Apra S10 (nM)	erlotinib hydrochloride (nM)
EC68	0.35	8960
EC46	0.32	2410
PANC-1	2.75	13100

Table 2.

Summary statistics for the pharmacokinetic parameters on the observed concentration-time profiles.[a]

	Tissue	Plasma		Pancreas		Liver		Lung		Brain		Salivary gland		Spleen		Kidney	
	Route	IV	IP	IV	IP	IV	IP	IV	IP	IV	IP	IV	IP	IV	IP	IV	IP
K_e	1/h	0.089	0.082	0.059	0.051	0.056	0.067	0.041	0.023	0.009	0.006	0.048	0.024	0.027	0.031	0.077	0.036
$t_{1/2}$	h	7.78	8.50	11.70	13.49	12.46	10.28	16.95	29.93	78.84	116.95	14.46	29.33	25.37	22.22	9.03	19.34
T_{max}	h	0.17	0.17	8.00	3.00	0.17	0.17	0.17	0.17	0.17	0.17	1.00	3.00	8.00	0.17	0.17	1.00
C_{max}	ng/mL	1072	775	2348	2883	1127	945	329	210	63	18	1258	556	195	253	753	403
AUC_t	ng*h/mL	1287	1251	45982	54532	6095	7485	2273	2321	874	727	23604	13009	4686	5011	3285	4508
AUC	ng*h/mL	1303	1292	49289	60205	6560	7951	2768	3310	2442	3067	26182	19233	6838	6586	3345	5559
MRT	h	4.20	6.54	14.80	17.46	14.08	12.77	24.55	38.38	110.88	170.68	19.56	41.75	38.00	31.38	9.34	25.57
CL/F	mL/(h*kg)	768	774	20	17	152	126	361	302	409	326	38	52	146	152	299	180
Vz/F	mL/kg	8616	9490	342	323	2741	1865	8837	13044	46571	55015	797	2200	5353	4868	3892	5020

[a]See Methods section for the definitions of PK parameters.